Int. J. Heat Mass Transfer. Vol. 29, No. 5, pp. 703–712, 1986
Printed in Great Britain

0017–9310/86 $3.00 + 0.00
Pergamon Journals Ltd.

Large Rayleigh number convection in a horizontal, eccentric annulus containing saturated porous media

K. HIMASEKHAR* and HAIM H. BAU

Department of Mechanical Engineering and Applied Mechanics, University of Pennsylvania, 111A Towne Building/D3, Philadelphia, PA 19104, U.S.A.

(*Received* 11 *June* 1985 *and in final form* 15 *November* 1985)

Abstract—Large Rayleigh number thermal convection in a horizontal, eccentric annulus containing a saturated porous medium is studied using a boundary-layer technique. The results include a description of the flow and temperature fields as well as a correlation for the Nusselt number as a function of the Rayleigh number, the radii ratio and the eccentricity. The latter correlation is valid for all Rayleigh numbers as long as the flow is two-dimensional, bicellular, and steady. The results obtained here are compared and favorably agree with numerical simulations and with experimental data.

1. INTRODUCTION

BUOYANCY-induced convection in porous media is germane to many technologies involving thermal insulators such as steam lines, gas lines in gas-cooled nuclear reactors, cryogenics, and storage of thermal energy. The thermal insulator typically consists of a fibrous material, which is permeable to fluid motion. Consequently, natural convection may develop in the insulating material. Caltagirone [1], Burns and Tien [2], Brailovskaya *et al.* [3], and others have demonstrated that the convective mode contributes significantly to the heat transfer process. Recently, Bau [4, 5] and Bau *et al.* [6] showed that under certain conditions eccentric insulators may be more economical than the commonly used concentric ones. The eccentric insulators may be more efficient than the concentric ones since the heat transfer in the insulation consists of both natural convection and conduction. An increase in the eccentricity, such that the center of the inner, hotter cylinder is above the center of the outer one, reduces the effective Rayleigh number and therefore the impact of the convective heat transfer. On the other hand, the resulting reduction in the local thickness of the insulation may increase the conductive heat losses. Hence, one may expect that an optimal value of eccentricity exists with which the heat losses are minimized.

In refs. [4] and [5], Bau used a regular perturbation expansion to solve analytically the Darcy–Oberbeck–Boussinesq equations and to construct a relationship between the Nusselt and Rayleigh numbers. The resulting series had a limited radius of convergence. Consequently, the results were limited to low Rayleigh numbers. The range of utility of the series was extended to moderate Rayleigh numbers [5] using a variety of non-linear transformations. In ref. [6], the same problem was solved numerically, and the theoretical calculations were confirmed qualitatively through comparison with flow visualization experiments. The numerical scheme becomes unstable, however, for large values of the Rayleigh number.

From the foregoing, it is apparent that the problem of large Rayleigh number convection in an eccentric annulus has not been resolved as yet. The objective of this manuscript is to procure a description of the flow and temperature fields as well as a relationship between the Nusselt and the Rayleigh numbers for large Rayleigh number flow. To this end, we use boundary-layer theory. The annulus is divided into boundary layer and core regions, and the governing equations are simplified accordingly. The boundary-layer equations are solved using an integral technique. The procedure used here is similar to the ones devised by Simpkins and Blythe for a rectangular cavity containing Newtonian fluid [7] and porous media [8], and Jischke and Farshchi [9] for a horizontal, concentric annulus containing Newtonian fluid. The temperature and flow fields so obtained are compared with numerical solutions. The results also are used to construct a correlation between the Nusselt and the Rayleigh numbers which is valid for all Rayleigh numbers.

2. MATHEMATICAL MODEL

Consider a saturated porous medium confined between two eccentric cylinders of radii r_i and $r_o > r_i$ (Fig. 1). The line connecting the center of the two cylinders is parallel to the gravity vector ($-g\hat{e}_z$). The distance between the cylinders' centers (the eccentricity, e) is denoted as positive when the center of the inner cylinder is above the center of the outer cylinder. The cylinders' surfaces are impermeable and maintained at

* On study leave from the Department of Mechanical Engineering, Andhra University, Waltair, 530003 India.

NOMENCLATURE

a, b numerical constants
d characteristic dimension of the porous medium
e eccentricity
$\hat{\mathbf{e}}_x$ unit vector in the horizontal direction
$\hat{\mathbf{e}}_z$ unit vector in the vertical direction
g gravitational acceleration
k equivalent thermal conductivity of the saturated porous medium
$\hat{\mathbf{n}}$ unit vector normal to the surface
Nu_{BL} Nusselt number predicted by boundary-layer theory, equation (29)
Nu Nusselt number
p pressure
Pr Prandtl number, ν/α
Q_c conductive heat flow in the absence of convection
Q_t total heat flow
r radius
R the radii ratio, r_o/r_i
Ra Darcy–Rayleigh number, $\lambda g\beta(T_i-T_o)r_i/(\nu\alpha)$
Re Reynolds number
T temperature
u_c velocity scale, $g\beta(T_i-T_o)\lambda/\nu$
v velocity
x horizontal coordinate
y coordinate along the cylinder's axis
z vertical coordinate.

Greek symbols
α equivalent thermal diffusivity of the porous medium
β thermal expansion coefficient of the saturating fluid
Δ thickness of the boundary layer
θ nondimensional temperature, $(T-T_o)/(T_i-T_o)$
λ permeability
μ fluid viscosity
ν kinematic viscosity of the saturating fluid
ξ stretched coordinate
ϕ azimuthal coordinate
ψ streamfunction.

Subscripts
c core variable
i inner cylinder (also, inner boundary-layer variables)
o outer cylinder (also, outer boundary-layer variables)
p plume variables
r radial velocity
ϕ angular component
x horizontal component
z vertical component
CL centerline

constant uniform temperatures, T_i and $T_o < T_i$, respectively. As a result of the above temperature difference, fluid motion is induced in the medium.

We assume that the fluid motion can adequately be described by steady, two-dimensional, Darcy–Oberbeck–Boussinesq (DOB) equations. The range of validity of the above assumptions is discussed later in the paper. The DOB equations, written in non-dimensional form, are

$$\nabla\cdot\mathbf{v} = 0 \tag{1a}$$

$$\mathbf{v} = -\nabla p + \theta\hat{\mathbf{e}}_z \tag{1b}$$

$$Ra\,\mathbf{v}\cdot\nabla\theta = \nabla^2\theta \tag{1c}$$

where the Darcy–Rayleigh number $Ra = g\beta(T_i-T_o)\lambda r_i/\nu\alpha$; the velocity scale $u_c = g\beta(T_i-T_o)\lambda/\nu$; the pressure scale is $\mu u_c r_i/\lambda$; the temperature $\theta = (T-T_o)/(T_i-T_o)$; the length scale is r_i; $\mathbf{v}$ is the Darcian velocity; p is the pressure deviation from the hydrostatic pressure; and $\hat{\mathbf{e}}_z$ is a unit vector in the vertical direction. The significance of the other symbols is given in the Nomenclature.

The corresponding boundary conditions are

$$\begin{aligned} &\theta = 1 \quad \mathbf{v}\cdot\hat{\mathbf{n}} = 0 \quad \text{on the inner surface } (r = 1)\\ &\theta = 0 \quad \mathbf{v}\cdot\hat{\mathbf{n}} = 0 \quad \text{on the outer surface } (r = R) \end{aligned} \tag{2}$$

and the symmetry condition at the vertical axis ($x = 0$, Fig. 1) is

$$\frac{\partial\theta}{\partial x} = v_x = 0.$$

In the above, $R = r_o/r_i$ is the radii ratio, and $\hat{\mathbf{n}}$ is a unit vector normal to the cylinders' surfaces.

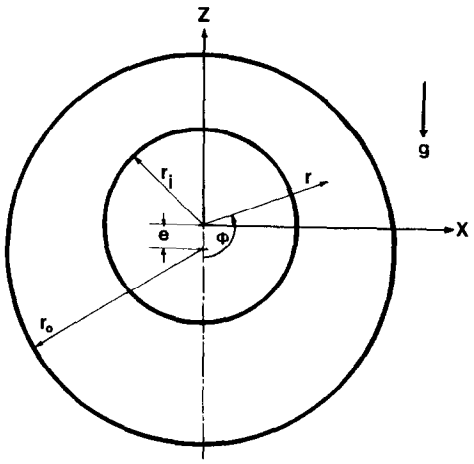

FIG. 1. The geometrical configuration.

In this paper we discuss explicitly the case of the inner cylinder being hotter than the outer one ($T_i > T_o$). The formulation as well as the results also apply to the case of the inner cylinder being colder than the outer one ($T_i < T_o$). In the latter case, the eccentricity will be denoted as positive if the center of the inner cylinder is below the center of the outer cylinder.

3. BOUNDARY-LAYER FORMULATION

Experimental observations as well as numerical simulations [6] suggest that, for high Rayleigh numbers, the fluid flow domain can be divided into five regions (Fig. 2).

(i) *Inner boundary layer*: a thin thermal layer near the inner cylinder in which gradients in the azimuthal direction are negligible compared to those in the radial direction.
(ii) *Outer boundary layer*: another very thin thermal layer near the outer cylinder.
(iii) *Plume*: exists along the vertical line of symmetry above the inner cylinder and joins the inner and outer thermal layers. (The inner boundary refurnishes the outer one through the plume.)
(iv) *Stagnant region*: a region, located beneath the inner cylinder, in which the buoyancy forces inhibit fluid motion and heat transfer takes place largely by conduction.
(v) *Core region*: which is bounded by the other four regions described above. The outer boundary layer empties into the inner one through the core region.

A similar classification of the various flow regions was done by Jischke and Farshchi [9] for the case of a concentric annulus containing a Newtonian fluid.

We find it convenient to analyze the various regions mentioned above by using local coordinate systems (Fig. 1), i.e. radial coordinates for the inner and outer boundary layers and Cartesian coordinates for the plume and the core regions. First, we estimate the thickness of the boundary layers to be $O(Ra^{-1/2})$ so that convection is balanced by radial conduction. The above is true for both the inner and outer boundary layers as long as the radii ratio R is not too large. The velocity attains its largest value in the boundary layer, where according to the momentum equation, the angular velocity is $O(1)$.

Next, we simplify the governing equations (1) for the asymptotic limit of large Rayleigh numbers.

(i) *The core region*

Since the azimuthal velocity in the boundary layer is $O(1)$, the continuity equation suggests that the entrainment velocity should be $O(Ra^{-1/2})$. The core empties the outer boundary layer and fills the inner one with fluid. Consequently, the core velocity should also be $O(Ra^{-1/2})$. Next, we denote the core variables with subscript c and retain terms of $O(1)$ only. The governing equations (1) assume the following form:

$$\nabla \cdot v_c = 0 \tag{3a}$$

$$\nabla p_c = \theta_c \hat{\mathbf{e}}_z \tag{3b}$$

$$\mathbf{v}_c \cdot \nabla \theta_c = 0 \tag{3c}$$

where all the variables $\mathbf{v}_c = Ra^{1/2}\,\mathbf{v}$, $p_c = p$ and $\theta_c = \theta$ are $O(1)$.

Taking a curl of the core-momentum equation (3b) we obtain:

$$\text{curl}\,(\theta_c \hat{\mathbf{e}}_z) = \frac{\partial \theta_c}{\partial x}\,\hat{\mathbf{e}}_y = 0 \tag{4}$$

where x is the horizontal coordinate, and y is parallel to the cylinders' axis. Thus, we conclude that $\theta_c = \theta_c(z)$, i.e. the core is stratified. From the core energy equation (3c), we conclude that the vertical component of the core velocity is zero, i.e.

$$\mathbf{v}_c = v_{c,x}\hat{\mathbf{e}}_x. \tag{5}$$

Further, the continuity equation (3a) suggests that $\partial v_{c,x}/\partial x = 0$, which implies that the horizontal velocity is a function of the vertical coordinate only [i.e. $v_{c,x} = v_{c,x}(z)$]. Thus when the Rayleigh number approaches infinity, the core velocity field, in the first approximation, is horizontal, and so are the streamlines, $\psi_c = Ra^{1/2}\psi$. This agrees well with the experimental observations and the numerical simulations ([6] and Fig. 2).

(ii) *The inner boundary layer*

When we analyze the inner boundary layer, we employ a local, cylindrical coordinate system centered at the center of the inner cylinder. Further, we rescale the various variables so that all variables in the inner boundary layer are $O(1)$. The inner boundary layer variables are denoted with a subscript i. The boundary-layer coordinate normal to the inner cylinder's surface

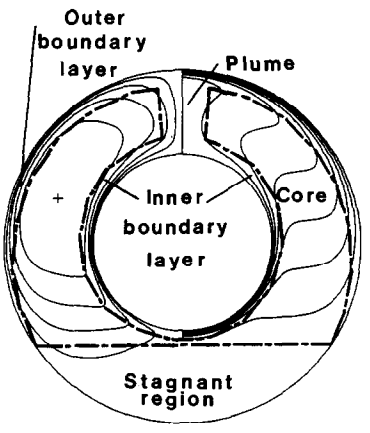

FIG. 2. The flow field (LHS) and the temperature field (RHS) as obtained from a finite-difference numerical simulation for a concentric annulus of radii ratio $R = 2$ and $Ra = 1000$. The heavy dashed lines indicate the division into the various flow regimes employed in the boundary-layer analysis.

$\xi_i = Ra^{1/2}(r-1)$, the radial velocity $u_{i,r} = Ra^{1/2}u_r$, and the streamfunction $\psi_i = Ra^{1/2}\psi$.

Next, we substitute the boundary-layer variables into the governing equations and retain terms of $O(1)$ only to obtain:

$$\frac{\partial u_{i,r}}{\partial \xi_i} + \frac{\partial u_{i,\phi}}{\partial \phi_i} = 0 \tag{6a}$$

$$u_{i,\phi} = -\frac{\partial p}{\partial \phi_i} + \theta_i \sin \phi_i \tag{6b}$$

$$0 = -\frac{\partial p}{\partial \xi_i} \tag{6c}$$

$$u_{i,r}\frac{\partial \theta_i}{\partial \xi_i} + u_{i,\phi}\frac{\partial \theta_i}{\partial \phi_i} = \frac{\partial^2 \theta_i}{\partial \xi_i^2}. \tag{6d}$$

The momentum equation in the ξ_i direction (6c) suggests that the pressure inside the boundary layer is the same as the pressure in the core region. Consequently,

$$u_{i,\phi} = (\theta_i - \theta_c)\sin \phi_i \tag{7}$$

The corresponding boundary conditions are:

$$\begin{aligned} &\xi_i = 0 \quad u_{i,r} = 0 \quad \theta_i = 1 \\ &\xi_i \to \infty \quad u_{i,\phi} \to 0 \quad \theta_i \to \theta_c. \end{aligned} \tag{8}$$

(iii) *The outer boundary layer*

In analyzing the outer boundary layer, we employ a cylindrical coordinate system centered at the center of the outer cylinder. The analysis proceeds along similar lines to that carried out for the inner boundary layer. The resulting equations are:

$$\frac{\partial u_{o,r}}{\partial \xi_o} + \frac{1}{R}\frac{\partial u_{o,\phi}}{\partial \phi_o} = 0 \tag{9a}$$

$$u_{o,\phi} = (\theta_o - \theta_c)\sin \phi_o \tag{9b}$$

$$u_{o,r}\frac{\partial \theta_o}{\partial \xi_o} + \frac{u_{o,\phi}}{R}\frac{\partial \theta_o}{\partial \phi_o} = \frac{\partial^2 \theta_o}{\partial \xi_o^2} \tag{9c}$$

with the boundary conditions

$$\begin{aligned} &\xi_o = 0 \quad u_{o,r} = \theta_o = 0 \\ &\xi_o \to \infty \quad u_{o,\phi} \to 0, \quad \theta_o \to \theta_c. \end{aligned} \tag{10}$$

In the above, subscript o denotes variables associated with the outer boundary layer. The coordinate normal to the surface $\xi_o = Ra^{1/2}(R-r)$, $u_{o,r} = -Ra^{1/2}u_r$ and $\psi_o = Ra^{1/2}\psi$.

(iv) *The plume*

According to experimental observations and numerical simulations [6], the inner boundary layer fills the outer one with fluid through a plume centered on the vertical axis above the inner cylinder. The plume is relatively thin and one may expect that the gradients in the horizontal direction are much larger than those in the vertical direction.

For convenience, we employ, in the plume region, a Cartesian coordinate system (x, z). Considerations of mass conservation dictate that the thickness of the plume should be the same as the thickness of the boundary layer, i.e. $O(Ra^{-1/2})$. We proceed by rescaling the various variables so as to bring them to $O(1)$. The plume variables are denoted with subscript p. Thus, the horizontal variable $\xi_p = Ra^{1/2}x$, $u_{p,x} = Ra^{1/2}u_x$, $u_{p,z} = u_z$, $\psi_p = Ra^{1/2}\psi$, etc. Next, we substitute the rescaled terms of $O(1)$ to obtain:

$$\frac{\partial u_{p,x}}{\partial \xi_p} + \frac{\partial u_{p,z}}{\partial z_p} = 0 \tag{11a}$$

$$u_{p,z} = (\theta_p - \theta_c) \tag{11b}$$

$$u_{p,x}\frac{\partial \theta_p}{\partial \xi_p} + u_{p,z}\frac{\partial \theta_p}{\partial z_p} = \frac{\partial^2 \theta_p}{\partial \xi_p^2} \tag{11c}$$

with the boundary conditions

$$\begin{aligned} &\xi_p = 0 \quad u_{p,x} = \frac{\partial u_{p,z}}{\partial \xi_p} = \frac{\partial \theta_p}{\partial \xi_p} = 0 \\ &\xi_p \to \infty \quad u_{p,z} \to 0, \quad \theta_p \to \theta_c. \end{aligned} \tag{12}$$

(v) *The stagnant region*

In the first-order theory presented here the stagnant region does not play any role.

4. SOLUTION PROCEDURES

In the previous section, we derived simplified governing equations for each of the flow regimes. These equations are coupled and none of them can be solved independently. An approximate solution can be devised using an integral technique [7–9]. We proceed by first deriving the integral form of the conservation equations in the various regimes. Next, we assume various shapes of velocity and temperature profiles in the boundary layers and the plume. These profiles are required to satisfy both the boundary conditions and the conservation laws in their integral form. That is, in effect, we convert the integro-differential equations into ordinary differential equations, which can be integrated with relative ease.

(i) *Inner boundary layer*

The integrated inner boundary-layer equations have the form:

$$\psi_c = \int_0^\infty u_{i,\phi}\, d\xi_i = \int_0^\infty (\theta_i - \theta_c)\sin \phi_i\, d\xi_i \tag{13a}$$

$$\frac{d}{d\phi_i}\int_0^\infty (\theta_i - \theta_c)^2 \sin \phi_i\, d\xi_i + \psi_c \frac{d\theta_c}{d\phi_i} = -\left(\frac{d\theta_i}{d\xi_i}\right)_{\xi_i = 0} \tag{13b}$$

We assume that the temperature profile can adequately be described by:

$$\theta_i - \theta_c = A_i(\phi_i)F_i\left[\frac{\xi_i}{\Delta_i(\phi_i)}\right], \tag{14}$$

where $\Delta_i(\phi_i)$ measures the thickness of the inner boundary layer and $F_i(\zeta)$ describes the shape of the

velocity profile. Substitution of (14) into (13) yields:

$$\psi_c \frac{d\theta_c}{d\phi_i} + a_i \frac{d}{d\phi_i}[\psi_c(1-\theta_c)] = -[b_i(1-\theta_c)^2 \sin\phi_i]/\psi_c, \tag{15}$$

where

$$a_i = \frac{1}{F_i(0)}\int_0^\infty F_i^2(\zeta)\,d\zeta, \quad b_i = \frac{F_i'(0)}{F_i^2(0)},$$

$$A_i(\phi_i) = \frac{1-\theta_c}{F_i(0)}, \quad \text{and} \quad \Delta_i(\phi_i) = \frac{F_i(0)\psi_c}{(1-\theta_c)\sin\phi_i}.$$

The form of $A_i(\phi_i)$ above ensures that equation (14) satisfies the boundary condition, $\theta = 1$, at the inner cylinder's surface.

The function $F_i(\zeta)$ is required to satisfy the normalization condition $\int_0^\infty F_i(\zeta)\,d\zeta = 1$; the boundary conditions at infinity, $F_i(\infty) = F_i'(\infty) = F_i''(\infty) = \cdots = 0$; and those at the inner cylinder's surface, $F_i''(0) = 0$.

(ii) *Outer boundary layer*

In analyzing the outer boundary layer, we employ a technique similar to the one employed in the inner boundary layer to obtain:

$$\psi_c \frac{d\theta_c}{d\phi_o} - a_o \frac{d}{d\phi_o}[\theta_c\psi_c] = -b_o \frac{\theta_c^2 R \sin\phi_o}{\psi_c}, \tag{16}$$

with

$$a_o = \frac{1}{F_o(0)}\int_0^\infty F_o^2(\zeta)\,d\zeta \quad \text{and} \quad b_o = \frac{F_o'(0)}{F_o^2(0)}.$$

The function $F_o(\zeta)$ is required to satisfy similar conditions to those satisfied by $F_i(\zeta)$.

(iii) *Plume*

The integral form of the conservation equations (11) is

$$\psi_c = \int_0^\infty u_{p,z}\,d\xi_p = \int_0^\infty (\theta_p - \theta_c)\,d\xi_p$$

$$\psi_c \frac{d\theta_c}{dz_p} + \frac{d}{dz_p}\int_0^\infty (\theta_p-\theta_c)^2\,d\xi_p = 0. \tag{17}$$

We assume that the temperature profile can be approximated in the form

$$\theta_p - \theta_c = A_p(z_p)G[-\xi_p/\Delta_p(z_p)] \tag{18}$$

where $\Delta_p(z_p)$ measures the half-width of the plume. Substitution of (18) into (17) leads to

$$\psi_c \frac{d\theta_c}{dz_p} + a_p \frac{d}{dz_p}[\psi_c(\theta_{CL}-\theta_c)] = 0 \tag{19}$$

where θ_{CL} is the temperature at the axis ($\xi_p = 0$). Note that a new variable (θ_{CL}) is introduced in equation (19). Consequently, an additional equation is needed. To this end, we substitute (18) into equation (11c), which was evaluated at $\xi_p = 0$, to obtain

$$\frac{d\theta_{CL}}{dz_p} + b_p \frac{(\theta_{CL}-\theta_c)^2}{\psi_c^2} = 0 \tag{20}$$

where

$$a_p = \frac{1}{G(0)}\int_0^\infty G^2(\zeta)\,d\zeta, \quad b_p = -G''(0)/G^3(0).$$

$$\Delta_p(z_p) = G(0)\psi_c/(\theta_{CL}-\theta_c),$$

and

$$A_p(z_p) = (\theta_{CL}-\theta_c)/G(0).$$

The function $G(\zeta)$ satisfies the normalization condition $\int_0^\infty G(\zeta)\,d\zeta = 1$ and the boundary conditions $G'(0) = G''(0) = 0$, $G(\infty) = G'(\infty) = G'''(\infty) = \cdots = 0$.

Initial and matching conditions

Before we proceed any further, it is convenient to rewrite the equations in terms of the global vertical coordinate z. For the inner and outer cylinders, $z = -\cos\phi_i$ and $z = -R\cos\phi_o - e$, respectively. Thus equations (15) and (16) become:

$$\psi_c \frac{d\theta_c}{dz} + a_i \frac{d}{dz}[\psi_c(1-\theta_c)] = -\frac{b_i(1-\theta_c)^2}{\psi_c}, \quad -1 \leqslant z \leqslant 1 \tag{21}$$

$$\psi_c \frac{d\theta_c}{dz} - a_o \frac{d}{dz}[\psi_c\theta_c] = -b_o \frac{\theta_c^2}{\psi_c}, \quad -1 \leqslant z \leqslant R-e. \tag{22}$$

In order to integrate equations (19)–(22), adequate initial conditions need to be specified. The continuity of temperature and streamfunction require that

$$\psi_c = \theta_c = 0 \quad \text{at} \quad z = -1.$$

This initial condition is of little use since equations (21) and (22) are singular at $z = -1$. Asymptotic analysis reveals that

$$\left.\begin{aligned} \psi_c &\sim \left(-2\frac{b_i}{a_i}\right)^{1/2}(1+z)^{1/2} \\ T_c &\sim C\psi_c^{a_i/(1-a_i)} \end{aligned}\right\} \quad \text{for} \quad z \to -1^+ \tag{23}$$

where C is an arbitrary constant. With some loss of generality, we assume in the above that $a_i = a_o$ and $b_i = b_o$. Thus, by selecting a value for C, one can simultaneously integrate equations (21) and (22) for $-1 < z < 1$. We shall specify later how C should be selected.

In the region $1 < z < R-e$, equation (21) is replaced with equations (19) and (20). The previous solutions of (21) and (22) provide the values of ψ_c and θ_c at $z = 1$. However, since a new variable, θ_{CL}, is introduced, an additional initial condition is needed. The value of θ_{CL} at $z = 1$ is determined by requiring that the thermal energy carried by the inner boundary layer at $z = 1^-$ will be equal to that carried by the plume at $z = 1^+$, i.e.

$$\int_0^\infty u_{i,\phi}(\theta_i - \theta_c)\,d\xi_i = \int_0^\infty u_{p,z}(\theta_p - \theta_c)\,d\xi_p. \tag{24}$$

In terms of the corresponding temperature profiles, we obtain

$$\theta_{CL}(z=1^+)=\frac{a_i}{a_p}+\left(1-\frac{a_i}{a_p}\right)\theta_c(z=1^-). \quad (25)$$

At this point, the equations can be integrated for any given value of C. In order to determine the value of C, we require that the point at which the plume intercepts the outer surface be a stagnation point. That is,

$$u_{p,z}=0 \quad \text{or} \quad \theta_{CL}=\theta_c \quad \text{at} \quad z=R-e. \quad (26)$$

Thus, the solution strategy for a given radii ratio (R) and eccentricity (e) is to select C, integrate the equations, obtain the value of $u_{p,z}$ at $z=R-e$, and, if that is not zero, change the guess for C and keep iterating until $u_{p,z}$ $(z=R-e)=0$ is satisfied. Alternatively, one may choose C, integrate the equations until the point at which $u_{p,z}=0$, and find the corresponding $R-e$. Note that R and e do not appear independently, but only as the combination $(R-e)$.

The heat transfer

Once the equations are solved, the heat flux and the total heat flow can be readily calculated. The total heat flow (Q_t) can be expressed as:

$$Q_t=2Ra^{1/2}\int_{-1}^{1}\frac{(1-\theta_c)^2}{\psi_c}\,dz. \quad (27)$$

The conductive heat flow (Q_c), in the absence of convection, is

$$Q_c=2\pi\left[\log R+\log\frac{m+\sqrt{(m^2-1)}}{\sqrt{(m^2-1)}+\sqrt{(m^2+R^2-1)}}\right]^{-1} \quad (28)$$

where $m=(R^2-e^2-1)/2e$. Consequently, the Nusselt number (Nu_{BL}) predicted by the boundary-layer theory is:

$$Nu_{BL}=Q_t/Q_c \quad (29)$$

The velocity and temperature profiles

In our calculations, we employ similar functions for the temperature profile in the inner and outer boundary layers, i.e. $F_i=F_o=F$. The various profiles used and the corresponding values of the constants $a_i=a_o=a$ and $b_i=b_o=b$ are given in Table 1. Additionally, we calculate Q_t for the special case of $R\to\infty$. The latter corresponds to the case of a cylinder imbedded in an infinite porous medium. This case is singled out both for its practical importance and for the availability of approximate solutions in the literature [10] with which we can compare our results. For example, Cheng [10] calculated the heat flow associated with a cylinder imbedded in an infinite medium. By neglecting the radial component of the gravity vector, he was able to construct a similarity solution. His result is quoted as the last entry in Table 1.

As is evident from Table 1, the actual values of a and b are not very sensitive to the selection of a specific profile F. The exponential profile $F(\zeta)=\exp(-\zeta)$ leads to the best agreement with Cheng's [10] solution and therefore it was used in our subsequent calculations.

For the plume, we use the profile [9]:

$$G(\xi_p)=\frac{2}{\sqrt{\pi}}\cos(\xi_p)\exp[0.25-\xi_p^2] \quad (30)$$

which results in $a_p=0.7293$ and $b_p=1.4291$.

The numerical integration

Equations (19)–(22) are integrated using a fourth-order accurate Runge–Kutta technique. As we indicated earlier, we start the integration process by guessing the value of C and subsequently calculating the location $(R-e)$ at which plume velocity terminates. The integration procedure cannot start at $z=-1$ since equations (21) and (22) have a singularity there. Consequently, the integration should begin at the point $z=-1+\varepsilon$, where $\varepsilon>0$ is typically taken to be 4×10^{-4}. Sensitivity analysis reveals that the end result is not affected when ε is varied by as much as two orders of magnitude.

The results of the computations are summarized in Fig. 3 where C is depicted as a function of $(R-e)$.

5. RESULTS AND DISCUSSION

5.1. *Temperature and velocity fields*

The core temperature (θ_c) and streamfunction (ψ_c) are depicted in Figs. 4 and 5 as functions of the vertical

Table 1. Values of a, b and $Q_t(R\to\infty)$ obtained for various temperature profiles $F(\zeta)$

$F(\zeta)$	a	b	$\frac{Q_t}{\sqrt{Ra}}$ for $R\to\infty$
1. $\exp(-\zeta)$	0.5	−1	2.828
2. $\frac{1}{3}(2+\zeta)\exp(-\zeta)$	0.5417	−0.75	3.399
3. Two-layer profile [8] $\frac{8}{9}-\frac{4}{7}\zeta+\frac{4}{63}\zeta^3;\ 0\leqslant\zeta\leqslant1$ $\frac{8}{21}\exp(-\zeta+1)\ \zeta>1$	0.5376	−1.7232	3.448
4. Ref. [10]	—	—	2.513

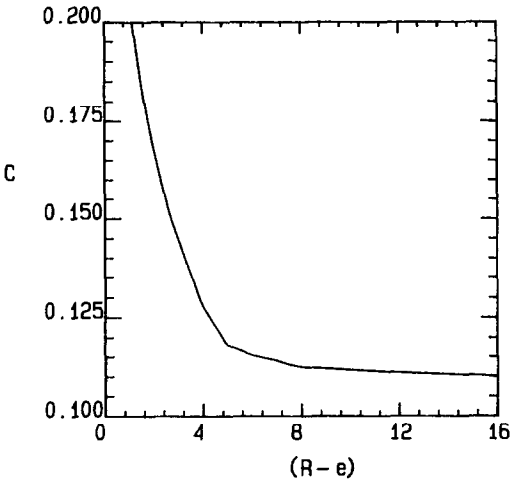

FIG. 3. The variation of the constant C as a function of $(R-e)$.

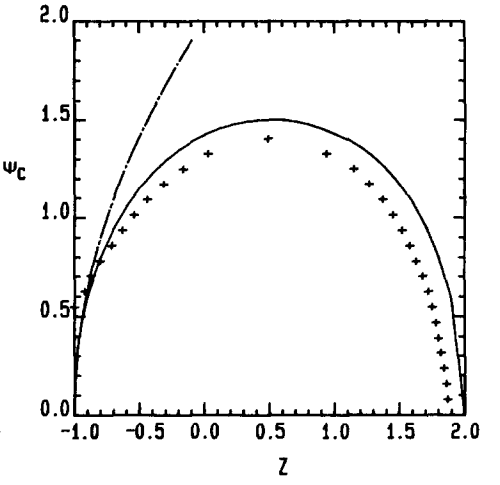

FIG. 5. The variation of the core stream function (ψ_c) as a function of the vertical coordinate (z) for a concentric annulus of radii ratio $R = 2$. The solid lines correspond to the boundary-layer solution, the dashed lines represent the asymptotic solution valid for $z \to -1^+$, and the symbols are the results of a finite difference numerical simulation for $Ra = 1000$.

coordinate (z) for a concentric annulus ($e = 0$) with radii ratio $R = 2$. The solid lines represent the results obtained by integrating equations (19)–(22). The dashed lines represent the asymptotic solution for $z \to -1^+$ [equation (23)], and the symbols represent the finite-difference numerical solution of the DOB equations (1) for $Ra = 1000$ [6]. Note the qualitatively good agreement between the boundary-layer solution (solid lines) and the numerical simulation (symbols). The core streamfunction (Fig. 4) starts from a zero value at $z = -1$, attains a maximum at about $z = 0.5$, and decreases back to zero at $z = R = 2$. The core temperature θ_c (Fig. 5) starts from zero at $z = -1$ and increases monotonically with z. At $z = R = 2$, it attains the same value as the plume's centerline temperature.

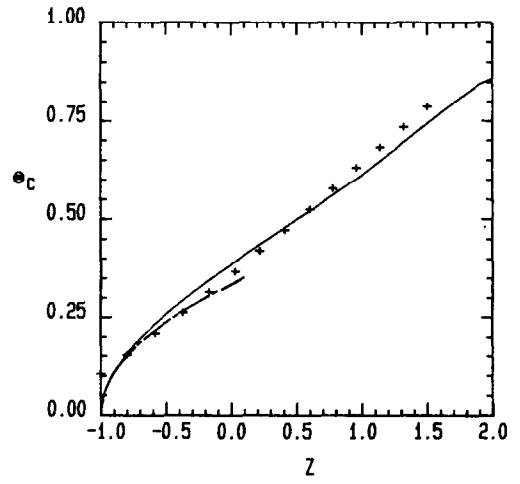

FIG. 4. The variation of the core temperature (θ_c) as a function of the vertical coordinate z for a concentric annulus with radii ratio $R = 2$. The solid line corresponds to the boundary-layer solution, the dashed line represents the asymptotic solution valid for $z \to -1^+$, and the symbols are the results of a finite-difference numerical simulation for $Ra = 1000$.

The core temperature (θ_c) never reaches the temperature ($\theta = 0$) of the outer surface.

We note in passing that an exact relationship between ψ_c and θ_c can be obtained for $-1 < z < 1$ in the form

$$C\psi_c^{a/(1-a)} = \theta_c(1-\theta_c). \tag{31}$$

Equation (31) is in excellent agreement (not shown here) with the results depicted in Figs. 4 and 5. We did not find an explicit analytical solution for $\theta_c = \theta_c(z)$ and $\psi_c = \psi_c(z)$ for general values of a and b.

5.2. *Heat transfer*

Next, we use the boundary-layer theory in order to calculate the Nusselt number Nu_{BL} as a function of the Rayleigh number [equation (29)]. The results are depicted as dashed lines in Figs. 6–9. In Fig. 6, we show the results for a concentric annulus with radii ratios $R = 2^{1/4}$, $2^{1/2}$, 2, 4 and 16. The symbols represent the results of a finite-difference numerical simulation [1]. The agreement between the boundary-layer theory and the numerical simulation is very good for $Nu_{BL} > 1.4$. In Fig. 7, we compare the Nu_{BL} with experimental data obtained by Caltagirone [1] for a concentric annulus of radii ratio $R = 2$. Note the good agreement between the boundary-layer theory and the experimental observations for $1.4 < Nu_{BL} < 2$. For higher values of the Nusselt number, the deviation between the experimental data and the theoretical results increases. The reason for this deviation will be discussed in the next section.

In Figs. 8 and 9 we depict the Nusselt number as a function of the Rayleigh number for eccentric annuli with positive and negative eccentricities, respectively.

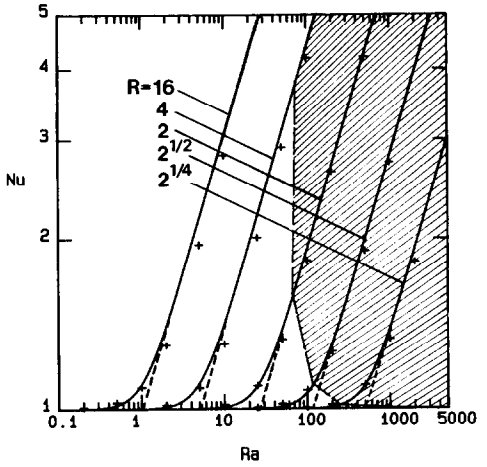

FIG. 6. The Nusselt number (Nu) depicted as a function of the Rayleigh number (Ra) for a concentric annulus of radii ratios $R = 2^{1/4}$, $2^{1/2}$, 2, 4 and 16. The solid line represents the uniformly valid correlation [equation (33)], the dashed line corresponds to the results of the boundary-layer theory, and the symbols represent numerical data from ref. [1]. The shaded area corresponds to a region in which the flow is not two-dimensional.

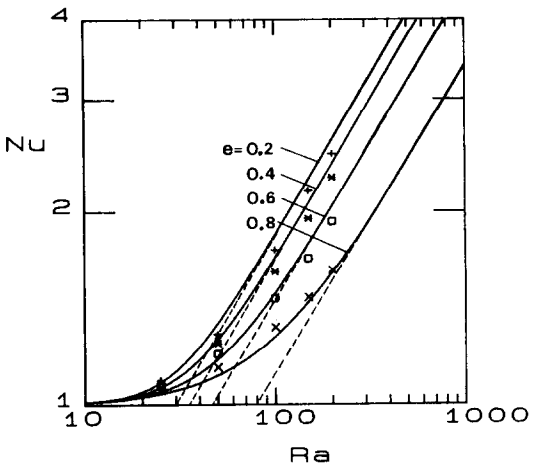

FIG. 8. The Nusselt number (Nu) as a function of the Rayleigh number (Ra) for an eccentric annulus of radii ratio $R = 2$ and eccentricity $e = 0.2, 0.4, 0.6$ and 0.8. The solid and dashed lines represent, respectively, the uniformly valid correlation (33) and the boundary-layer theory. The symbols represent numerical solution [6].

The various symbols are the results of two-dimensional, finite-difference numerical simulation [6]. The agreement between the boundary-layer theory and the numerical simulation is very good for $|e| \leqslant 0.6$. As the eccentricity increases, however, the numerical data starts deviating from the boundary-layer results. Note that for $|e| > 0.6$, the gap between the outer and inner cylinders becomes very small. Thus, the deviation between the numerical simulation [6] and the boundary-layer theory may be attributed to the fact that the Rayleigh numbers for which we possess numerical data [6] are not sufficiently large to ensure distinct inner and outer layers.

The results obtained for the boundary-layer theory and the results of the numerical simulation were used to construct a correlation for the heat flow Q_t in the form:

$$Q_t = 2\pi\, Ra^{1/2}\{0.35 - 0.11 \exp[-0.39(R - e - 1)]\}. \tag{32}$$

The above value of Q_t can be used to calculate Nu_{BL} in

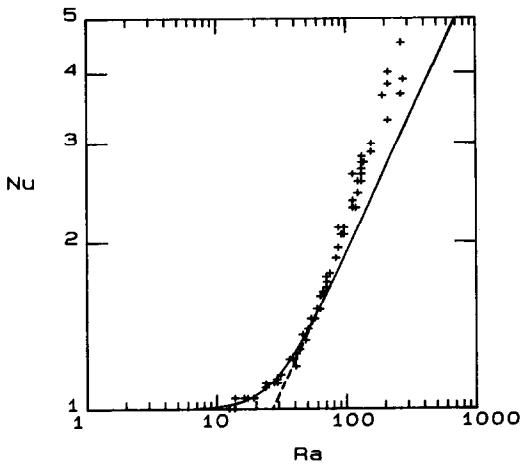

FIG. 7. The Nusselt number (Nu) as a function of the Rayleigh number (Ra) for a concentric annulus of radii ratio $R = 2$. The solid and dashed lines represent respectively the uniform correlation (33) and the boundary-layer theory. The symbols represent experimental data [1].

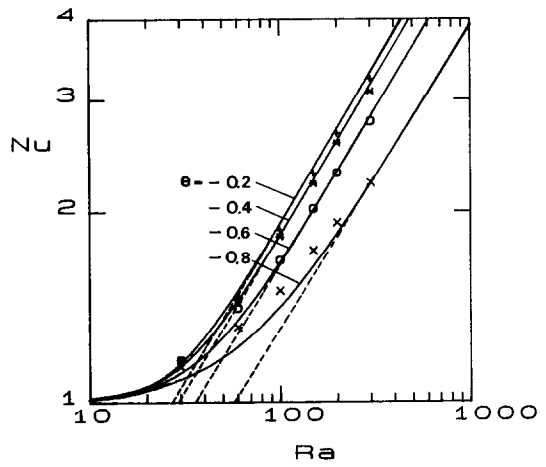

FIG. 9. The Nusselt number (Nu) as a function of the Rayleigh number (Ra) for an eccentric annulus of radii ratio $R = 2$ and eccentricities $e = -0.2, -0.4, -0.6$ and -0.8. The solid and dashed lines represent, respectively, the uniformly valid correlation (33) and the boundary-layer theory. The symbols represent numerical solutions [6].

accordance with equation (29). At this point, we possess the asymptotic limits for the Nusselt number for large and small Rayleigh numbers, i.e. as $Ra \to 0, Nu \to 1$ and as $Ra \to \infty, Nu \to Nu_{BL}$. Using a technique devised by Churchill and Usagi [11], the above two limits can be used to construct an approximation for all Rayleigh numbers in the form:

$$Nu = (1 + Nu_{BL}^{6-4.5e^2})^{1/(6-4.5e^2)}. \quad (33)$$

The results obtained using this correlation are depicted by solid lines in Figs. 6–9. The deviation between (33) and the numerical data is smaller than 8% for all the cases examined.

6. THE RANGE OF VALIDITY OF THE RESULTS

The theoretical results presented here are based on the assumption that the flow is two-dimensional and steady. This is the case only for certain values of the Rayleigh number. Once a certain critical value of the Rayleigh number is exceeded, the flow becomes three-dimensional and oscillatory. For the case of the concentric annulus, we use Caltagirone's results [1] to show the region (shaded) in Fig. 6, in which the flow is not two-dimensional. Unfortunately, similar data for the eccentric annulus is not available yet. The bifurcation into three-dimensional convection also explains why beyond a certain Rayleigh number the experimental data in Fig. 7 starts deviating from the theoretical results. Clearly, correlation (33) is not valid in the three-dimensional convective regime (shaded area in Fig. 6). Nevertheless, the correlation (33) can provide a lower bound for the heat transfer in the three-dimensional flow regime.

Another matter of concern is the validity of the DOB equations for large Rayleigh numbers. Darcy's law is considered to be valid for Reynolds numbers $Re < 10$, where $Re = \bar{u}_c d/\nu$. In the foregoing equation, d is a characteristic dimension of the porous media (i.e. pore or particle diameter) and $\bar{u}_c$ is the Darcian velocity. In our case, the maximum velocity is attained in the boundary layer and can be estimated from $\bar{u}_c = \lambda g\beta(T_i - T_o)(1-\theta_c)/\nu F(0)$. Consequently, we conclude that the DOB equations are valid for

$$Ra < 20\, Pr \frac{r_i}{d} \quad (34)$$

where Pr is the Prandtl number. For example, in the case of air ($Pr \sim 0.7$) and $r_i/d \sim 10^2$, the DOB equations will be valid for $Ra < 1400$.

7. CONCLUSION

A boundary-layer technique was used to solve for the temperature and flow field as well as for the heat transfer in an eccentric horizontal annulus containing saturated porous media. The results agree favorably with numerical simulations and with experimental observations and enable us to construct a heat transfer correlation which is valid in the range of validity of the DOB equations and as long as the convective motion remains two-dimensional, bicellular and steady.

Acknowledgment—This material is based upon work supported by the National Science Foundation under Grant Nos. MEA-8217565 and MEA83-51658.

REFERENCES

1. J. P. Caltagirone, Thermoconvective instabilities in a porous medium bounded by two concentric horizontal cylinders, *J. Fluid Mech.* **76,** 337–362 (1976).
2. P. J. Burns and C. L. Tien, Natural convection in porous medium bounded by concentric spheres and horizontal cylinders, *Int. J. Heat Mass Transfer* **22,** 929–939 (1979).
3. V. A. Brailovskaya, G. B. Petrazhitskii and V. I. Polezhaev, Natural convection and heat transfer in porous interlayers between horizontal coaxial cylinders, *J. appl. Mech. tech. Phys.* **19,** 781–785 (1978).
4. H. H. Bau, Low Rayleigh number thermal convection in a saturated porous medium bounded by two horizontal, eccentric cylinders, *Trans. Am. Soc. mech. Engrs*, Series C, *J. Heat Transfer* **106,** 166–175 (1984).
5. H. H. Bau, Thermal convection in a horizontal eccentric annulus containing a saturated porous medium—an extended perturbation expansion, *Int. J. Heat Mass Transfer* **27,** 2277–2287 (1984).
6. H. H. Bau, G. McBlane and I. Saferstein, Numerical simulation of thermal convection in an eccentric annulus containing porous media, ASME 83-WA/HT-34 (1983).
7. P. A. Blythe and P. G. Simpkins, Thermal convection in a rectangular cavity. In *Physico-Chemical Hydrodynamics* (edited by D. B. Spalding), Vol. 2, pp. 511–524. Advance (1977).
8. P. G. Simpkins and P. A. Blythe, Convection in a porous layer, *Int. J. Heat Mass Transfer* **23,** 881–887 (1980).
9. M. C. Jischke and M. Farshchi, Boundary layer regime for laminar free convection between horizontal circular cylinders, *Trans. Am. Soc. mech. Engrs*, Series C, *J. Heat Transfer* **102,** 228–235 (1980).
10. Ping Cheng, Natural convection in a porous medium: external flows, Presented at NATO Advanced Study Institute, July 16–27 (1984).
11. S. W. Churchill and R. Usagi, A general expression for the correlation of rates of heat transfer and other phenomena, *A.I.Ch.E. Jl* **18,** 1121 (1972).

CONVECTION A GRAND NOMBRE DE RAYLEIGH DANS UN ESPACE ANNULAIRE EXCENTRIQUE, HORIZONTAL ET CONTENANT UN MILIEU POREUX SATURE

Résumé—La convection thermique à grand nombre de Rayleigh dans un espace annulaire excentrique, horizontal, contenant un milieu poreux saturé, est étudiée à l'aide d'une technique de couche limite. Les résultats contiennent une description des champs d'écoulement et de température aussi bien qu'une expression du nombre de Nusselt en fonction du nombre de Rayleigh, du rapport des rayons et de l'excentricité. L'expression est valable pour tous les nombres de Rayleigh tant que l'écoulement est bidimensionnel, bicellulaire et permanent. Les résultats obtenus ici sont comparés et ils s'accordent avec les solutions numériques et avec les données expérimentales.

KONVEKTION BEI GROSSEN RAYLEIGH-ZAHLEN IN EINEM HORIZONTALEN, EXZENTRISCHEN RINGRAUM, WELCHER GETRÄNKTE PORÖSE MEDIEN ENTHÄLT

Zusammenfassung—Die thermische Konvektion in einem waagerechten, exzentrischen Ringraum, welcher ein durchtränktes poröses Medium enthält, wird mit Hilfe einer Grenzschicht-Technik für den Fall großer Rayleigh-Zahlen untersucht. Die Strömungs- und Temperaturfelder werden beschrieben, außerdem wird eine Korrelation der Nusselt-Zahl in Abhängigkeit von der Rayleigh-Zahl, vom Verhältnis der Radien und von der Exzentrizität mitgeteilt. Letztere Korrelation ist für alle Rayleigh-Zahlen gültig, solange die Strömung zweidimensional, bizellular und stationär ist. Die vorgelegten Ergebnisse werden mit numerischen Simulationeu und mit Versuchsdaten verglichen, wobei sich eine recht gute Übereinstimmung ergibt.

КОНВЕКЦИЯ ПРИ БОЛЬШИХ ЧИСЛАХ РЭЛЕЯ В ГОРИЗОНТАЛЬНОМ ЭКСЦЕНТРИЧЕСКОМ КОЛЬЦЕВОМ КАНАЛЕ, СОДЕРЖАЩЕМ НАСЫЩЕННУЮ ПОРИСТУЮ СРЕДУ

Аннотация—В приближении пограничного слоя изучается тепловая конвекция при больших числах Рэлея в горизонтальном эксцентрическом кольцевом канале, содержащем насыщенную пористую среду. Найдены поля скорости и температуры и выражение для числа Нуссельта как функции числа Рэлея, отношения радиусов и эксцентриситета. Указанное выражение справедливо в том диапазоне чисел Рэлея, в котором течение является двумерным, двухячеистым и устойчивым. Полученные результаты хорошо совпадают с численными расчетами и экспериментальными данными.